SPE 93429

The Impact of Faults Representation on History Match and Future Generated Seismic Impedance Response in Reservoir Models—Case Study for Pierce Field, North Sea

B. Al-Busafi, SPE, Q.J. Fisher, SPE, S.D. Harris, and M. Kendall, U. of Leeds

This paper was prepared for presentation at the SPE Europec/EAGE Annual Conference held in Madrid, Spain, 13-16 June 2005.

Abstract

Transmissibility multipliers provide a simple way of accounting for the effects that faults have on fluid flow in production simulation models. Recent studies have shown that transmissibility multipliers can be quantified from parameters such as fault thickness and permeability (Knai and Knipe, 1998; Manzocchi *et al.*, 1999). Generally, these latter parameters must be approximated using empirical relationships with some host rock properties such as V-shale or net-to-gross ratio as well as fault displacement magnitude (Manzocchi *et al*., 1999).

In this study, the effects of two different representations of faults on the history match and the predicted (simulated) seismic impedance are compared for the **Pierce Field**, **North Sea**. In the first case, fault transmissibilities were adjusted and the faults were extended in a trial and error manner to improve the match to fluid contacts and production history. In the second case, a step-by-step derivation of the fault transmissibilities in the Pierce Field was adopted based upon the integration of collected and upscaled properties of the deformed and undeformed reservoir as well as empirical relationships between fault offset and thickness. Historical production data were used to compare the effectiveness of the two methods. Furthermore, a synthetic seismic impedance response was generated from both simulation models, using a velocity model based on the Gassmann-Biot theory of elastic wave propagation in fluid saturated porous solid (Gassmann, 1951; Biot, 1956). This allows the assessment of different fault representations when trying to predict optimal times for further time-lapse seismic surveys. The results demonstrate the effectiveness of the derived transmissibilities model in generating a satisfactory history match in a relatively short time period. The generated seismic models show that, by acting as baffles/barriers to fluid flow, faults can play a major role in creating residual seismic features that can be observed on 4D seismic surverys. Incorporating realistic fault rock properties into the simulation model, which is used to create synthetic seismic, can therefore allow geophysicists and engineers to better plan the timing of 4D seismic surveys so that they have the greatest influence on field development decisions.

Introduction

After a production simulation model has been constructed, it must be tested to determine whether it can reproduce the previous production behavior (*i.e.* fluid flow rates, pressures *etc.*) of the reservoir. Modelling past performance will identify weakness in the input parameters to the model, suggest possible modifications and demonstrate the quality of the reservoir description that is eventually accepted before future reservoir performance is modelled. In structurally complex reservoirs (*e.g.* densely faulted), history matching can be a time-consuming and frustrating process due to the large number of parameters that affect performance. Indeed, history matches are inevitably non-unique and therefore the best efforts should be made to ensure that all input parameter are physically/geologically realistic. New technologies are providing increased amounts of data that allow this non-uniqueness in the history match to be reduced. For example, time-lapse (4D) seismic surveys can be used to place more constraints on the fluid flow behavior of reservoirs (Greaves *et al.,* 1987). To use time lapse seismic effectively, acquisition and processing must be as similar as possible for each survey in the series to ensure that differences can be related to production effects and not merely survey artifacts. The power of this technique lies in its ability to map fluid movements in the lateral and vertical space of the reservoir thus enabling reservoir engineers to locate unswept zones. Of particular interest for the present study is possibility that time-lapse seismic can sometimes be used to identify the presence of sealing faults (Lumley and Behrens, 1998; Koster and Gabriels, 2000).

Most benefit from a 4D is gained if the timing between the two seismic acquisitions coincides with a period in field development that the results are likely to have a significant

effect on well planning. Oil companies aim to gain time-lapse seismic with big residual impedance response in the shortest possible time in order to achieve an early, reliable, reservoir model description. Due to changes in production and injection strategies with time, or non-linear mechanical compaction within the reservoir, the magnitude of the expected impedance residuals may not be proportional to the length of time since production begins. Initial reservoir models, with acceptable history matches, can be used to predict the timing for optimum forthcoming acquisition by creating a synthetic acoustic impedance response from the fluid flow information. Such initial assessment can be a vital step in quantifying a company's business objectives.

In this work, the effects of fault representation in creating residual seismic features are addressed. Two models of the Pierce Field, North Sea were used. The two reservoir models are similar apart from how the fault properties were derived. In the first case, fault transmissibility multipliers (TMs) were adjusted and the faults were extended in a trial and error manner to improve the match to fluid contacts and production history. In the second case, a step-by-step derivation of the fault transmissibilities in the Pierce Field was adopted based upon the integration of upscaled properties of the host rock. To assess the reliability of the latter model, laboratory measurements of microstructural and petrophysical properties of fault rocks from a single well in the Pierce Field were conducted. Appropriate transmissibilities were derived from permeability and capillary pressure measurements.

An Overview of the Pierce Field Faults

Pierce Field, North Sea, is a highly faulted reservoir with radial and concentric faults (**Fig. 1**). It is located in UK blocks 23/22a and 23/27 in Central North Sea, approximately 265km from Aberdeen. The field comprises the two accumulations of Pierce North and Pierce South discovered 14 years apart by well UK 23/27-3 in 1976 and well UK 23/22a-2 in 1990. The field structure comprises two salt diapirs, which fully penetrate the reservoirs, giving structural dips of up to 70° adjacent to the diapers. An interesting aspect is the large variation in depth to the oil-water contact (OWC) across the field, varying 300m from west to east. The OWC surface dips to the west with an average gradient of 5° (90m/km). The original field development plan attributed the observed variations in OWC to the presence of sealing radial faults. Recent development drilling has indicated this early model to be largely incorrect. It has shown that most of the areas of South Pierce are in direct communication, and that most radial faults are not sealing; at worst they provide zones of reduced transmissibility. The only radial faults that have enough vertical displacement to seal (>200 ft) are those that overlie major NW-SE and NE-SW trending basement fault zones. However in common with other radial faults at Pierce, the displacements rapidly decrease away from the diapir, and it is considered that sealed compartments can only be formed in conjunction with concentric faults (which are far more laterally extensive than the radial faults) and/or stratigraphic trapping elements. It is possible that concentric faults are important, yet difficult to image, baffles to fluid flow within the Pierce Field. These faults accommodate most of the vertical strain involved in diapir growth, providing several hundred feet of vertical displacement at a low angle (or parallel) to the steeply dipping beds on the diapir flank. The largest concentric faults are interpreted as forming linked-fault systems, which produce a ring fault around much of the diapir, offset by large displacement radial faults. Such a combination of concentric and radial faults is most likely to create structurally isolated reservoir compartments high on a diapir flank, particularly in areas of the field characterised by a low net/gross reservoir.

The first Pierce full field simulation model was completed in September 2001. History match results, to November 2002, showed that the largest mismatches are in water cuts and observed well-bottom hole pressures. The major unknown parameter in the model is the fluid flow properties of the faults, which were incorporated as TMs. A review of RFT (Repeat Formation Tester) data confirmed the important role that faults play in the distribution of Pierce fluids. For example, development wells A1 and B2 (**Fig. 1**) both encountered differential depletion along their trajectory due to a pre-development extended well test. Volumetric analysis concluded that the regional aquifer overpressure gradient is modified locally by fault-related baffles, with possible further differences in free water level (FWL) observed between stratigraphic layers.

Measured or inferred OWC information was included in the geological model under a range of 18 different faulting scenarios. A probabilistic range of hydrocarbons in place was derived for each scenario, based on the property maps, and Monte Carlo analysis was used to generate the final range of volumetric results. The sensitivity of original hydrocarbons in place to OWC is greatest in the saddle region, between the two diapiric salt-abutment traps, where 100 ft depression of the contact gives an additional 30 MMstb of original oil in place.

Faults Transmissibility Representations

Transmissibility multipliers, are absolute numbers used routinely in simulation models to take into account the fluid flow properties of faults (Manzocchi *et al.,* 1999). TMs are calculated by dividing the transmissibility between grid cells with the fault taken into account by the transmissibility without the fault (**Equation 1**). The effective transmissibility between cells across the fault is computed by the simulator by multiplying the unfaulted transmissibility by the TM. Thus, totally sealing faults can be represented with $TM = 0$, and faults that do not affect fluid flow are assigned with $TM = 1$. In this section, two models for the Pierce Field (**Fig. 1**) are described. The first model was history matched by manually changing faults TMs until a satisfactory match was obtained. We refer to this model as 'old-fault TM' model. The second model involves fault TM derivation, using a method analogous to that outlined by Manzocchi *et al.* (1999), except it takes into account cell geometric factors when dealing with distorted corner point geometry. We refer to this model as 'new-fault TM' model. Sensitivity simulation studies were performed on the field to identify the faults that require more attention in their representation and special treatment. In this model, special treatment was performed on three faults,

numbered 1-3 in **Fig. 1,** as sensitivity studies showed that these faults could have relatively significant effects on history matches. The special treatment involves the implication of the multi-phase properties of faults within Pierce Field based on laboratory measurements, as will be discussed later. The model where no special treatment is performed and all faults are represented using the TM derivation is referred to as 'TM -Model'.

Old-Fault TM Model. Since the first history match, the transmissibility multipliers associated with faults within Pierce have been tuned and faults been extended to improve history match on a trial and error basis (**Fig. 1**). In all of the field simulation models, faults sealing magnitudes are independent of host -rock properties or depth, *i.e.,* the TM for each fault is the same whether the fault cuts water, oil or gas zones. Most of the faults in this model were represented as either completely sealing faults or completely open faults, with few faults with intermediate TMs (**Fig. 1**).

New-Fault TM Model. In this model, TMs were computed using the methodology of Manzocchi *et al.* (1999). To capture the static properties of fault zones using TMs, knowledge of both the permeability and thickness of the fault rock and the undeformed reservoir of the grid blocks immediately adjacent to the fault are required. The TM between two cells with permeabilities k_1 and k_2 juxtaposing a fault with thickness t_f and permeability k_f can be defined as a ratio between reciprocal of undeformed cells transmissibilities (T_1 and T_2) and the faulted cells transmissibilities (T_{1f} and T_{2f}):

$$TM = \frac{1/T_1 + 1/T_2}{1/T_{1f} + 1/T_{2f}}, \quad \textbf{(1)}$$

where for each cell *i* :

$$1/T_i = \frac{(1/2)d_i}{k_i A_i}, \quad \textbf{(2)}$$

$$T_{if} = a_i T_i, \quad \textbf{(3)}$$

$$a_i = \left[1 + \frac{t_f}{d_i}\left(\frac{k_i}{k_f} - 1\right)\right]^{-1}, \quad \textbf{(4)}$$

where A_i is contact area resolved for flow out of cell *i* and d_i is the magnitude of the vector joining centre of back face to centre of front face, with respect to the flow direction, of cell *i.*

In this study, fault thickness, t_f, was estimated from fault displacement using the harmonic average relationship of the observed data compiled by Hull (1988), and data from faults in mixed sandstone/shale sequences in Sinai (Knott *et al.,* 1996), SE Utah (Foxford *et al.,* 1998) and Lancashire, UK (Walsh *et al*., 1998a), see Manzocchi *et al*. (1999). The harmonic average of these data follow the relationship $t_f = d/170$, where d is the absolute fault displacement Fault permeability can be estimated based on the clay content of the fault zone (Fisher and Knipe, 2001). The clay content of the fault rock is estimated using algorithms such as Shale Gouge Ratio (SGR), which is the fraction of shale in the sequence that has passed each point on the fault (Yielding *et al*., 1997). The value for SGR for a single cell face can be found by summing up the effects of all other cells that have slid past that particular cell during faulting:

$$SGR = \frac{\sum V_{sh_i} \times D_i}{\sum D_i}, \quad \textbf{(5)}$$

where V_{sh_i} is the volume of shale (as a fraction) in grid cell$_i$ and D_i is the distance of the fault transport vector that crosses unit *i*. In this study V_{sh_i} was estimated from net/gross assuming that all rock volume in a cell that is not "Net" is "Shale". Such treatment gives the maximum shale content and therefore may result in an overestimation of the sealing capacity of faults.

The value of SGR is assumed to approximate the percentage of clay in the fault zone (Yielding *et al.,* 1997). Thus SGR can be converted to permeability using experimental determinations of permeability for fault gouges with varying clay content and appropriate geological history (see Manzocchi *et al.,* 1999; Sperrevik *et al.,* 2002). The calibration of Manzocchi *et al.* (1999) indicates that a fault gouge with clay content of *c*. 20% will be expected to have a single-phase permeability of between 0.03 and 0.3 mD. He approximated a relationship from an empirical prediction of fault zone permeability as a function of shale content and displacement. This relationship is given by the following equation:

$$\log k_f = A1 \times SGR - A2 \times \log(d_f) \times (1 - SGR)^{A3}, \quad \textbf{(6)}$$

where k_f is fault permeability (in mD) and d_f is fault displacement (in metres). *A1*, *A2*, and *A3*, are empirical constants fit to observed data, typically derived from outcrop and core data. In actual practice, it would be best to apply constant factors that are appropriate for the local field, play, or basin. Manzocchi *et al*. (1999), suggest values for *A1*, *A2*, and *A3* of -4, 0.25, and 5 respectively. In the permeability equation, the first term (*A1*) reflects permeability loss due to shale smear along the fault plane. The second term (*A2*) reflects permeability reduction due to non-smearing behaviour

(that is, for lithologies with low shale content). By modifying the constant terms, appropriate relations can be obtained that treat a variety of fault behaviours. For example, if fault permeability depends only on offset, then *A1* and *A3* are set equal to zero. In this study, those values suggested by Manzocchi *et al.,* (1999), were used to approximate fault permeability.

Fault rock thickness, SGR, permeability and transmissibility multipliers are shown in **Fig.2**. Fault face thickness takes a maximum value of 2.0 ft (corresponding to fault displacement of about 347 ft). As reflected in the fault thickness, fault displacement dies away when radiating away from the salt domes. Fault face transmissibility display shows that concentric faults appear to have a larger impact on fluid flow than radial faults as a result of the low net/gross around them. The average transmissibility multiplier of faults in Pierce Field is about 0.5. This figure indicates that these faults do not seem to have a large impact on fluid flows primarily owing to their small throws and low host rock permeabilities, which have an average of 10 mD.

Implication of the Microstructural and Petrophysical Faults Properties Measurements for Fluid Flow within Pierce Field. Microstructural and petrophysical faults properties measurements conducted during this study indicated that cataclasites are the main fault rock type in Pierce and have a geometric average permeability of 0.05 mD and a mean Hg-injection threshold pressure of 250 psi. The average permeability of the undeformed reservoir is around 10 mD. To take into account the presence of a 1 ft thick fault with this permeability within the aquifer in the production simulation model (the grid block width in the simulation model is 75 m) would require, according to equation **(1)**, a transmissibility multiplier of around 0.55 applied to the face of adjacent grid blocks. Assuming that the 250 psi Hg-threshold pressure converts to a threshold pressure of around 25 psi for the hydrocarbon-water system, these faults would be able to seal an oil column of 50 ft (Fisher *et al.,* 2001). In other words, the results from this study indicate that the faults would be totally sealing to oil for the first 50 ft directly above the free water level (FWL) within Pierce.

At higher levels above the FWL, we need to take into account relative permeability effects in calculating the transmissibility multipliers that need to be applied to take into account the presence of faults within Pierce. Unfortunately, there have not been any robust studies to measure the multi-phase flow properties of faults. As an alternative, we have used proprietary data on the end point relative permeabilities of low permeability rocks as well as the data from shales generated by Hildenbrand *et al.* (2002). The results are very consistent showing that rocks with low absolute permeabilities tend to have low relative permeabilities to gas at irreducible water saturation.

If we assume that once the capillary entry pressure of a fault rock is overcome (*i.e.* higher than 50 ft above the FWL) its water saturation will be at irreducible values, we can calculate relative transmissibility multipliers. The assumption regarding the lack of a transition zone within the fault will appear rather counterintuitive to most petrophysicists who are used to low permeability rocks having broad pore-size distributions. However, Hg-injection results indicate that cataclastic faults, as observed within this study, may differ in that they have a narrow range of pore-throat sizes, in which case the transition zone will be very thin. Based on these assumptions, we calculate a transmissibility multiplier of 0.4 would need to be applied to take into account the presence of faults within the oil and gas column of Pierce once the hydrocarbon column height is sufficient to overcome the capillary entry pressure of the fault rock.

In summary, the following parameters have been applied to take into account the presence of faults within the Pierce reservoir model (applied to faults numbered 1-3 in **Fig. 1**):

- A transmissibility multiplier of 0.55 was applied to take into account the presence of faults in the aquifer.
- A transmissibility multiplier of 0 was applied for the first 50 ft above the FWL to take into account the presence of a fault that is totally sealing to oil.
- A transmissibility multiplier of 0.4 was applied in the reminder of the hydrocarbon column to take into account the relative permeability of the fault rock.

History Match: Old-Fault TM Model versus New-Fault TM Model

History matches using the cumulative field gas, oil and water productions have been performed for both models to test their validities. In this study the history match was conducted using production data up until November 2003. **Fig. 3** and **Fig. 4** show that there is a dramatic improvement in history match using the 'new TM fault' model especially in the water and oil production data. The figure reveals an important observation about faults. The difference between the two models varies between the three phases with its maximum in water production and its minimum in gas production. In other words, faults in the Pierce Field have their biggest impact on water production whereas gas production is not sensitive to the range of faults transmissibilities applied during this study. Such behaviour can be attributed to the mobility ratios. In this model, gas is injected to displace oil. Due to its low viscosity, gas has a low mobility ratio and may easily flow across faults even if they have low-TMs. Water, on the other hand, covers a large area and has to pass several faults during the production process. Because faults are less transmissible in the water leg, especially in the low layers of the South and North Pierce (see **Fig. 2)**, the cumulative transmissibility to the water can become significant irrespective of its limited movements until this stage of the simulation.

Pierce Field Waterflooding Project and Future Prediction

To sweep basement oil, which is not accessed by the current gas re-injection scheme, nor swept by the weak aquifer, a waterflooding project was implemented on Pierce Field at the end of 2004. **Fig. 5** shows that by commencing the waterflooding project, the reservoir is re-energised with a pressure support. This pressure support will assist in limiting the producing GOR, preventing light-end hydrocarbons from falling out of solution, leading to high residual oil saturations, accelerating production as higher drawdowns become achievable and eliminating difficulties associated with

production start-up from low-pressure wells. At some point the water injection will be stopped and the gas caps (North and South) might be produced (gas cap blow-down).

In our study, seismic impedance changes are investigated based on changes in pressure and saturations at three different instances: before, during and after waterflooding, see **Fig. 3**. We refer to these instances of the production phases, indicated by grey circles in **Fig. 3**, as **stage 1** (start of the waterflooding project), **stage 2** (significant time after start of the waterflooding) and **stage 3** (after stopping the waterflooding project and producing and exporting the gas). The main focus is on which of the two parameters, *i.e.* pressure or water saturation, has more of an effect on creating residual seismic features around faults.

Generating Seismic Impedance Response from Simulation Models Output

Synthetic seismic impedance response was generated from both simulation models, using a velocity model based on the Gassmann-Biot theory of elastic wave propagation in fluid saturated porous solid (Gassmann, 1951; Biot, 1956). The aim was to assess the impact of fault representations on the timing of when to shoot further time-lapse seismic. The petroelastic model, part of the Geoquest ***ECLIPSE-100*** simulator has been used to generate the simulated acoustic impedance. The petroelastic model uses the Gassmann fluid substitution equations (Gassmann, 1951) to generate simulated seismic-derived quantities (such as acoustic impedance) in each active gridcell in a reservoir simulation model. The acoustic response of the reservoir is a combination of acoustic response of the different rocks and fluids that constitute the reservoir.

Velocity Model Theory. The effective acoustic response of the fluids is calculated from conventional simulation properties (such as pressure, fluid density, fluid saturations and effective porosities). The overall acoustic response of the reservoir is given by combining the effective acoustic response with the acoustic response of the rocks (both frame and minerals).

The use of the Gassmann fluid substitution equations in the petroelastic model relies on the following assumptions:

- The seismic frequencies used are sufficiently low (less than 100 Hz) such that the induced pore pressures are equilibrated throughout the pore space (that is there is sufficient time for the pore volume fluid to flow and eliminate wave-induced pore pressure gradients). This limitation to low frequencies explains why Gassmann's relation works best for very low frequency *in situ* seismic data (<100 Hz) and may perform less well as frequencies increase such as during sonic wire-line logging (~10^4 Hz) and laboratory ultrasonic measurements (~10^6 Hz)
- The rock is isotropic (i.e. the seismic wave speed is directional independent)
- There is a homogeneous elastic modulus for the minerals present.
- The fluid bearing rock is completely saturated.

In addition, the fluids are assumed to be not "too" viscous so that the shear stiffness of the reservoir is entirely due to shear stiffness of the dry rock frame.

In this paper, the impedance to pressure waves, I_p, is computed for every gridcell in the **Pierce Field** top layer. This is defined as:

$$I_p = \rho V_p , \qquad \textbf{(7)}$$

where ρ is the effective density of the composite material (fluids and minerals) in the gridcell and V_p is the effective **P**-wave velocity in the simulation gridcell. The effective velocities are calculated by:

$$V_p = \sqrt{\frac{K + (4G/3)}{\rho}} , \qquad \textbf{(8)}$$

where K is the effective bulk modulus of the simulation gridcell and G is the effective shear modulus of the simulation gridcell

The effective bulk modulus of the simulation gridcell is a combination of the effects of the fluids, the frame and the minerals in the gridcell.

The following form of Gassmann's equation is used in the petroelastic model:

$$K = K_{frame} + \frac{\left(1 - \frac{K_{frame}}{K_m}\right)^2}{\frac{\phi_{eff}}{K_{fluid}} + \frac{(1-\phi_{eff})}{K_m} - \frac{K_{frame}}{(K_m)^2}} , \qquad \textbf{(9)}$$

where K_{frame} is the effective bulk modulus of the dry rock frame for this gridcell, K_m is the effective bulk modulus of the minerals in this gridcell, K_{fluid} is the effective bulk modulus of the pore fluid in this gridcell and ϕ_{eff} is the effective porosity of this gridcell

With the assumption that the fluids in the gridcell are not too viscous, the overall shear modulus is just the shear modulus of the dry rock frame:

$$G = G_{frame} , \qquad \textbf{(10)}$$

where G_{frame} is the shear modulus of the dry rock frame for this gridcell

The effective density in a gridcell is given by the effective porosity weighted average of the fluid density and the mineral density in that gridcell:

$$\rho = \phi_{eff}.\rho_{fluid} + (1-\phi_{eff}).\rho_m, \quad (11)$$

where ρ_m is the effective density of the minerals in this gridcell and ρ_{fluid} is the effective density of the fluids in this gridcell

The effective density of the minerals is supplied directly as an input for each petroelastic region in the simulation model. Density of the minerals in the Pierce Field**,** as averaged from core sample measurements is, 2.65 g/cc.

The calculation of the effective porosity for a gridcell is based on the porosity at the reference pressure, ϕ_0, in the gridcell and the effects of rock compressibility or rock compaction (depending on which type of pressure effect is present in the model).

The petroelastic model uses a rock model that relates rock effective porosity, ϕ_{eff}, and compressibility by:

$$\phi_{eff} = \phi_0(1 + X + \frac{X^2}{2}), \quad (12)$$

where

$$X = C(P - P_{ref}), \quad (13)$$

and C, P and P_{ref} are the rock compressibility, the pressure and the rock compressibility reference pressure for each gridcell.

In each gridcell, the rock porosity and compressibility and their reference pressures and the pressure itself are available within the simulator.

The effective fluid density is the saturation weighted average of the individual fluid component densities:

$$\rho_{fluid} = S_o\rho_o + S_w\rho_w + S_g\rho_g, \quad (14)$$

where $S_{o,w,g}$ is the saturation of oil/water/gas in the gridcell and $\rho_{o,w,g}$ is the density of oil/water/gas in the gridcell. These quantities are available within the simulator for each gridcell.

There is a tendency for each phase to have a different induced pore pressure because the Pierce Field comprises multiple pore fluid phases with different fluid bulk moduli. Assuming that the phases are intimately mixed at the finest scale, these pore pressure increments can equilibrate with each other to a single average value. This is an isostress situation, and therefore the effective bulk modulus of the mixture of fluids is described well by the Reuss average (Reuss, 1929) as a saturation-weighted harmonic average of the individual fluid bulk moduli, that is

$$\frac{1}{K_{fluid}} = \frac{S_o}{K_o} + \frac{S_w}{K_w} + \frac{S_g}{K_g}, \quad (15)$$

where $K_{o,w,g}$ is the bulk modulus of the oil/water/gas in the gridcell determined by the phases densities and velocities.

Phase velocities are computed from the gridcell pressures and temperature using empirical relations similar to those summarized by Batzle and Wang (1992). The Pierce Field temperature varies due to large hydrocarbon column height and proximity to salt. RFT data indicate that the temperature is 245 degrees Fahrenheit, at the top of the reservoir with a gradient of 0.0171 degrees Fahrenheit/ft.

The rock moduli can often be predicted quite accurately by inserting this effective fluid modulus into Gassmann's relation. This approach has been discussed, for example, by Domenico, (1976); Murphy, (1984); Cadoret, (1993); as well as Mavko and Nolen-Hoeksema, (1994).

Results Discussion

The primary aim of this study was to investigate the effects of faults on the generated seismic impedance. This is a visual process aided with acoustic impedance maps generated from the velocity model described above. **Fig. 8** shows water saturation, pressure and P-wave impedance residual maps in three different instances during **stage 1**, **stage 2** and **stage 3**, see **Fig. 3**. These residual maps represent the differences between the old-fault TM model (**Fig. 6**) and the new-fault TM model (**Fig. 7**) at the corresponding stages. At the early stage of production and prior to the waterflooding project, the P-wave impedance residual map, **stage 1**, seems to have a good correlation with the pressure residual map (see **Fig. 8** top maps). There are obvious seismic features around faults in South Pierce. At this time there are abundant amount of compressible phases, *i.e.* oil and gas, which are capable of creating these seismic features even with little changes in reservoir pressure. For this reason, one can see that the seismic features are well correlated with the pressure residuals.

We predict in **stage 2** (significant time after start of the waterflooding), there are almost no seismic features created by faults irrespective of their representations (see **Fig. 8** middle maps). At this stage of the reservoir life, most of the gas and oil in the South Pierce and the saddle region between the two salt domes will have been swept by the flooded water (**Fig. 6** and **Fig. 7**, middle maps). The absence of the seismic features at this stage can be explained by phase distribution. The field water cut jumps from about 5% in **stage 1** to about 60% in **stage 2** (**Fig. 5**). The faults would be surrounded by the least compressible phase, water, except at the top of the salt domes. Although the pressure residual is larger than that in **stage 1**, the seismic features are far from being in correlation with the pressure distribution. The generated seismic impedance is almost identical for both faults representations at this stage, even though the residuals in pressure and saturations are greater than those in **stage 1** (**Fig. 8** middle maps).

In **stage 3** (after stopping the waterflooding project and producing and exporting the gas), a big drop in reservoir pressure takes place (**Fig. 6** and **Fig. 7**, bottom maps). In contrast, there is a small change in water saturation compared

to **stage 2**. This pressure drop allows the light-end hydrocarbons to come out of solution and gas features appear as it drops below its bubble point pressure (see saturation maps in **Fig. 6** and **Fig. 7** bottom maps). Looking at **stage 3** pressure residual map (**Fig. 8**, bottom maps) the North Pierce is dominated by negative pressure residual (light grey). The 'new-fault TM model' allows more pressure compartmentalisation in the North Pierce. On the other hand, the South Pierce is dominated by positive pressure residual (dark grey) meaning that the 'old-fault TM model' allows more pressure compartmentalisation in this part of the reservoir. This pressure residual is not well correlated with the P-wave impedance residual. There is, however, some degree of correlation in other parts of the reservoir.

Conclusions and recommendations

This study has lead to a number of conclusions and recommendations:

1. Fault rock laboratory data improved fault representations in simulation models at an early stage of reservoir life to gain early and reliable history matches.
2. Predicted seismics generated from simulation models can be used to plan the best timing for forthcoming seismic acquisition.
3. A new method for accounting for fault sealing capacities to petroleum cross flows based on their positions relative to the free water level has been presented and applied. The method uses some empirical relationships along with microstrucural and petrophysical fault properties calculations. The method demonstrated its ability in improving history match when applied to real and highly faulted reservoirs.
4. Faults representations can play an important role in creating seismic residuals that can be influential for geophysicists and reservoir engineers in planning their forthcoming seismic acquisition, even when these faults had a small impact on the history match to date.

Acknowledgements

The first author would like to thank Petroleum Development Oman (PDO) for funding this PhD research. The Pierce Field co-venturers: Shell U.K. Limited (operator), Oranje Nassau and MOEX, are acknowledged for granting permission to publish this paper. The author is very grateful to Sam Carter for acting as a focal communication point in Shell U.K. Limited throughout this work and for his constructive comments and suggestions.

References

1. Batzle, M., and Wang, Z. (1992). Seismic properties of pore fluids. *Geophys.*, **57**, 1396-1408.
2. Biot, M.A. (1956). Theory of propagation of elastic waves in a fluid saturated porous media. J. Appl. *Phys.*, **33**, 1482-1498.
3. Cadoret, T. (1993). Effect de la Saturation Eau/Gas sur les Propriétés Acoustiques des Roches. Ph.D dissertation, University of Paris, VII.
4. Domenico, S.N. (1976). Effect of brine-gas mixture on velocity in an unconsolidated sand reservoir. *Geophys.*, **41**, 882-894.
5. Fisher, Q.J., Harris, S.D., McAllister, E., Knipe, R.J. and Bolton, A.J. (2001). Hydrocarbon flow across sealing faults: theoretical constraints. *Marine and Petroleum Geology,* **18**, 251–257.
6. Foxford, K.A., Walsh, J.J., Watterson, J., Garden, I.R, Guscott, S.C., and Burley, S.D. (1998) "Structure and Content of the Moab Fault Zone, Utah, USA, and its Implications for Fault Seal Prediction", *Geological Society Special Publications*, **147**, 87-103
7. Gassmann, F., (1951). Über die Elastizität poröser Medien. *Vier. Der Natur. Gesellschaft in Zürich,* **96***, 1-23*
8. Greaves, R.J., and Fulp, T.J. (1987). "Three-dimentional seismic monitoring of an enhanced oil recovery process", *Geophysics*, **52**, 1175-1187.
9. Hildenbrand A., Schlömer, S., and Krooss, B.M., (2002) Gas breakthrough experiments on fine-grained sedimentary rocks. Geofluids, **2**, 3-23.
10. Hull, J. (1988). Thickness–displacement relationships for deformation zones. *Journal of Structural Geology*, **10**, 431–435.
11. Knai, T.A. & Knipe, R.J. (1998). The impact of faults on fluid flow in the Heidrun Field. In G. Jones, Q.J. Fisher, & R.J., Knipe. *Faulting and Fault Sealing and Fluid Flow in Hydrocarbon Reservoirs* (pp. 269-282). In *Special Publication of the Geological Society of London 147***.**
12. Knott, S.D., Beach, A., Brockband, P.J., Brown, J.L., McCallum, J.E., and Weldon, A.L. (1996). "Special and Mechanical Controls on Normal Fault Populations", *Journal of Structural Geology*, **18**, 359-372.
13. Koster, K., and Horvei, A. (2000) Reservoir monitoring of the Draugen field through time-lapse seismic and it's business impact. SPE 87300.
14. Lumley, D.E., and Behrens, R.A. (1998) Practical issues of 4D seismic reservoir monitoring: What an engineer needs to know. SPE *Reservoir Evaluation & Engineering*, December 1998, 528-538.
15. Manzocchi, T., Walsh, J.J., Nell, P. and Yielding, G. (1999). Fault transmissibility multipliers for flow simulation models. *Petroleum Geoscience,* **5**, 53–63.
16. Mavko, G., and Nolen-Hoeksema, R. (1994). Estimating seismic velocities in partially saturated rocks. *Geophys.*, **59**, 252-258.
17. Murphy, W.F., III, Winkler, K.W., and Kleinberg, R.L. (1984). Contact microphysiscs and viscous relaxation in sandstones, in *Physics and Chemistry of Porous Media*, D.L. Johnson and P.N. Sen, eds. *American Institute of Physics*, New Yourk, 176-190.
18. Reuss, A. (1929). Berechnung der Fliessgrenzen von Mischkristallen auf Grund der Plastizitätsbedingung für Einkristalle, *Zeitschrift für Angewandte Mathematik und Mechannik*, **9**, 49-58.
19. Sperrevik, S., Gillespie, P.A., Fisher, Q.J., Halvorsen, T. & Knipe, R.J. (2002). Empirical estimation of fault rock properties. In: Koestler, A.G. & Hunsdale, R. (eds) *Hydrocarbon Seal Quantification*. NPF Special Publication, **11**, Elsevier, Amsterdam.
20. Walsh, J.J., Watterson, J., Heath, A.E. & Childs, C. (1998a). Representation and sealing of faults in fluid flow models. *Petroleum Geoscience*, **4**, 241–251.
21. Yielding, G., Freeman, G., and Needham, B. (1997). "Quantitative Fault Seal Prediction", *American Association of Petroleum Geologists Bulletin*, **81**, 897-917.

SI Metric Conversion Factors

ft	× 3.048	E-01	=	m
Psi	× 6.894757	E+00	=	kPa
stb*	× 6.289808	E+00	=	sm^3
lb/ft^3	× 0.06242796	E+00	=	kPa
mD	× 9.869233	E-16	=	m^2
g/cc	× 1.00	E+03	=	kg/m^3
°F	× 33.800	E+00	=	°C

*Standard conditions are taken as one atmosphere and 60°F.

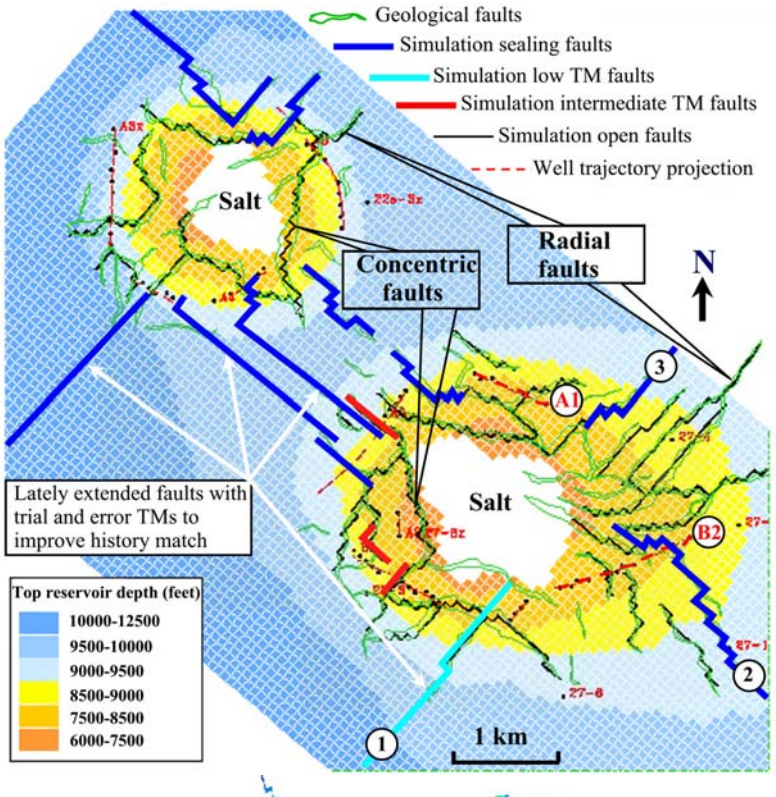

Fig. 1: The Pierce Field is located in UK blocks 23/22a and 23/27 in Central North Sea, approximately 265km from Aberdeen. Most of the faults in the field were simulated as open fault, with no resistance to flow (thin black lines). In this study, faults numbered 1-3 were given a special treatment and their sealing capacities were varied depending on their relative position with respect to the Free Water Level (FWL).

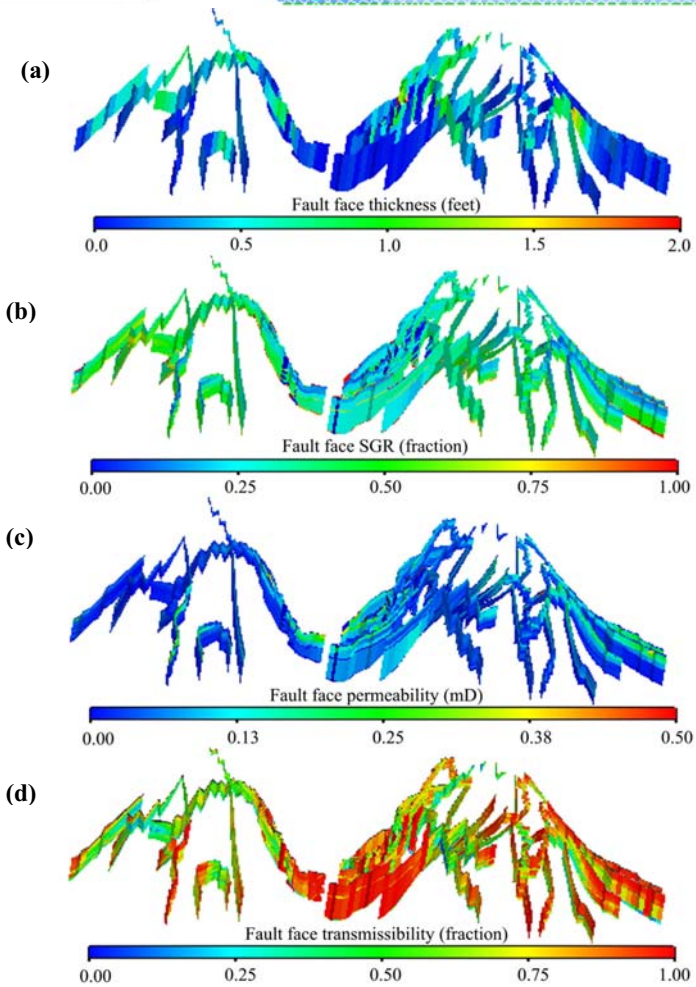

Fig. 2: (a) Fault face thickness, linearly derived from fault displacements. (b) Fault face SGR, derived from NTG ratio, which approximated the V-shale in the fault zone. (c) Fault face permeability, derived from fault thickness and SGR using using equation (7), see text. (d) Fault face transmissibility multiplier as derived from equation (1). The derivation follows the methodology of Manzocchi et al., 1999. Faults becom thinner when radiating away from the salt domes. Concentric faults (see Fig. 1) have less transmissibility than radial faults. Generally, radial faults become less transmissible with depth.

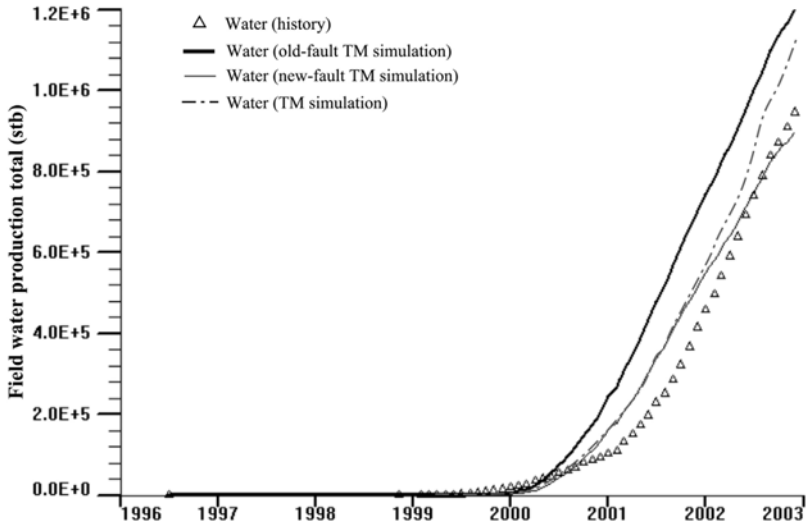

Fig. 3: Field water production total as a function of simulation time (in years). The 'old-fault TM Model' (thick solid line) represents the best history match resulting from extending the reservoir faults in using trial and error TMs. The 'new-fault TM Model' (thin solid line) represents the history match results using geologically-based derived TMs plus faults numbered 1-3 (see Fig. 1) were given a special treatment and their sealing capacities were varied depending on their relative position with respect to the Free Water Level (FWL). The 'TM Model' (thin dotted line) represents the history match results using geologically-based derived TMs

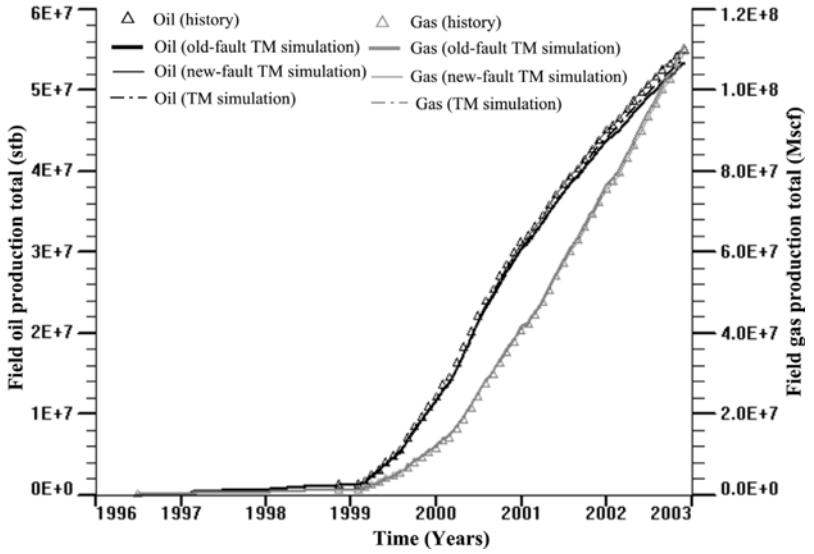

Fig. 4: Field oil and gas production totals as a function of simulation time (in years). The 'New-fault TM model' gives an excellent match with with observed data for the oil production. Faults do not have a clear impact on gas production because of the gas high mobility. Furthermore, most of the gas accumulation is around faults with high transmissibility multipliers (mostly in the top of the reservoir).

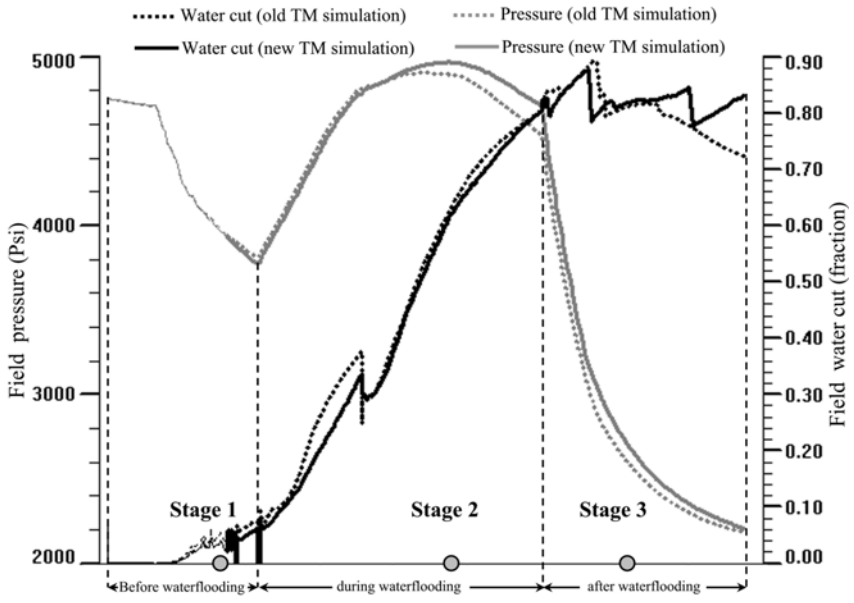

Fig. 5: Simulated field average pressure and water cut before, during and after commencing the waterflood project. The difference between the two models does not seem to be considerable in the long run. This study investigates if the impact is analogous on the future generated seismic properties. P-wave impedance maps are generated at three different stages (indicated by the grey circles) during the three phases of the reservoir production life.

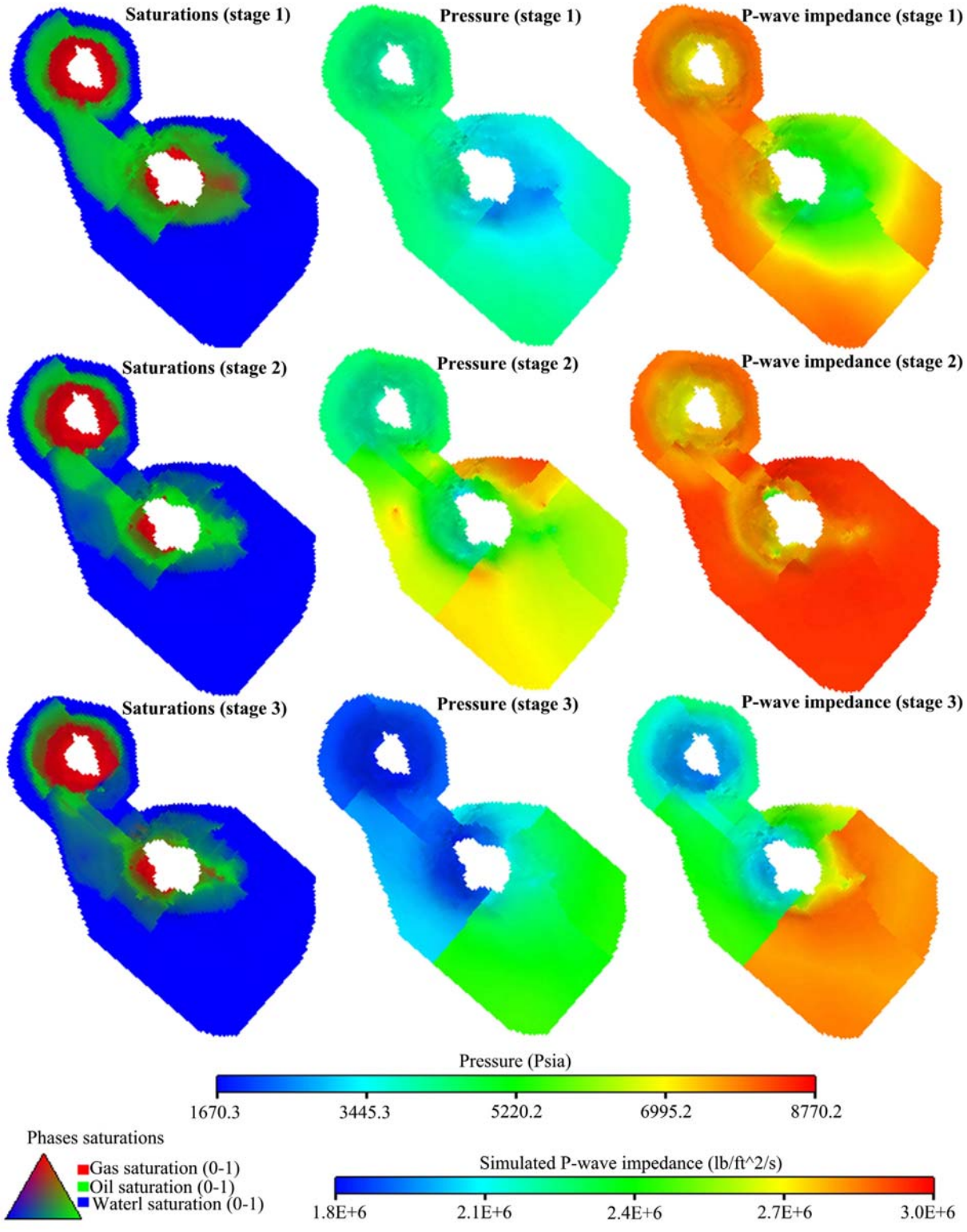

Fig. 6: Old-fault TM model results. Simulated phases saturations (left column), field pressure distribution (middle column) and P-wave impedance (right column) for stage 1 (start of the waterflooding project), stage 2 (significan time after start of the waterflooding) and stage 3 (after stopping the waterflooding project and producing and exporting the gas).

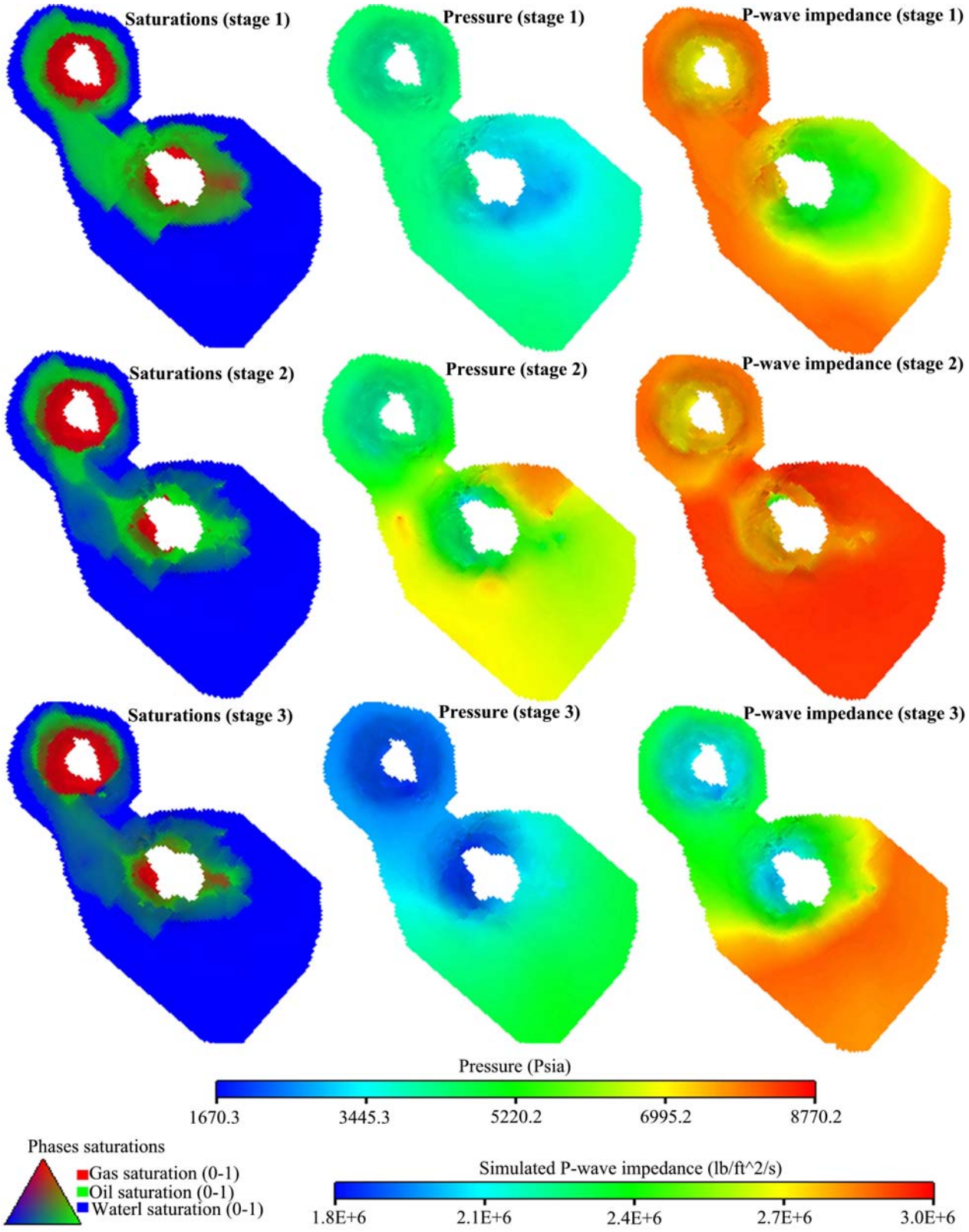

Fig. 7: New-fault TM model results. Simulated phases saturations (left column), field pressure distribution (middle column) and P-wave impedance (right column) for stage 1 (start of the waterflooding project), stage 2 (significan time after start of the waterflooding) and stage 3 (after stopping the waterflooding project and producing and exporting the gas).

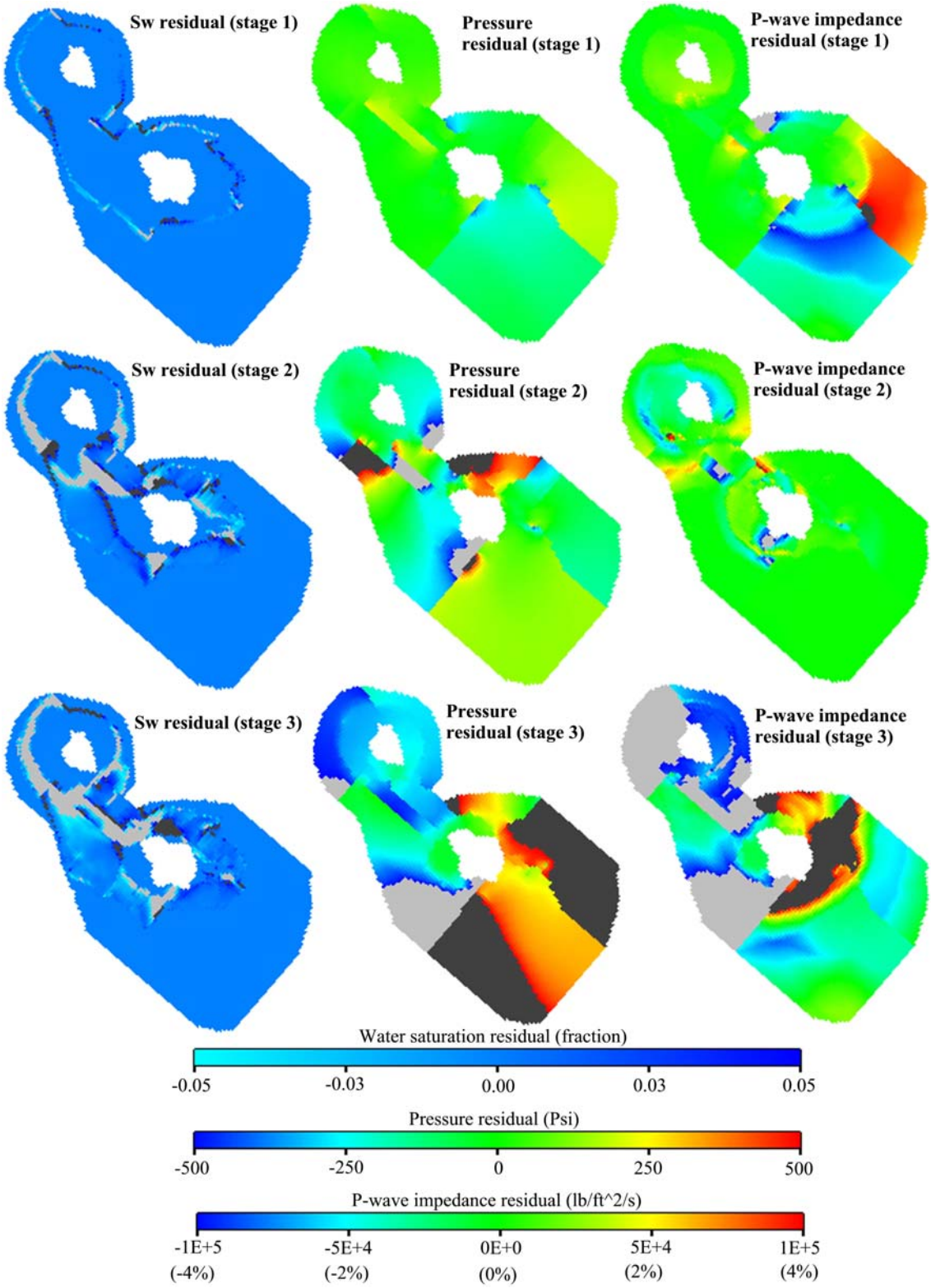

Fig. 8: Simulated phases saturations residuals (left column), field pressure distribution residuals (middle column) and P-wave impedance residuals (right column) for stage 1 (start of the waterflooding project), stage 2 (significan time after start of the waterflooding) and stage 3 (after stopping the waterflooding project and producing and exporting the gas). These residual maps represent the differences between the 'old-fault TM model' (Fig. 6) and the 'new-fault TM model' (Fig. 7) at the corresponding simulation times. Light grey colour represents the negative residuals beyond the shown scale, whereas the dark grey colour represents the positive residuals beyond the shown scales. These colours show the areas where the difference is extreme (*e.g.* > ±4% in the P-wave impedance residual).